REPORT DOCUMENTATION PAGE

Form Approved
OMB NO. 0704-0188

1. AGENCY USE ONLY (Leave Blank)	2. REPORT DATE	3. REPORT TYPE AND DATES COVERED
	Sep/03/2004	Final Report 03/15/2001 06/30/2004

4. TITLE AND SUBTITLE
Advanced Methods for Highly-Portable Field Repair Welding and Assessing Phase Stability and Aging of Alloys in Service

5. FUNDING NUMBERS
DAAD19-01-1-0375

6. AUTHOR(S)
David L. Olson and Yeong-Do Park

7. PERFORMING ORGANIZATION NAME(S) AND ADDRESS(ES)
Colorado School of Mines
Dept. Met. Mat. Engr.
Center for Welding, Joining, and Coating Research
Golden, Colorado 80401-1887

8. PERFORMING ORGANIZATION REPORT NUMBER
MT-CWJCR-004-027

9. SPONSORING / MONITORING AGENCY NAME(S) AND ADDRESS(ES)
U. S. Army Research Office
P.O. Box 12211
Research Triangle Park, NC 27709-2211

10. SPONSORING / MONITORING AGENCY REPORT NUMBER
41923.19-MS

11. SUPPLEMENTARY NOTES
The views, opinions and/or findings contained in this report are those of the author(s) and should not be construed as an official Department of the Army position, policy or decision, unless so designated by other documentation.

12 a. DISTRIBUTION / AVAILABILITY STATEMENT
Approved for public release; distribution unlimited.

20040914 050

13. ABSTRACT (Maximum 200 words)

New welding consumables and practices for weld repair are being investigated. Special attention was given to the repair of light metals (aluminum and magnesium alloys). Metal powder-filled cored aluminum wires to be used with microwire GMA spool hand held guns were being developed. The use of strip-to-wire mill to make powder metal-cored wires was being perfected as an effective methodology for making specialty alloy welding consumable wires. These wires are for repairing technical assemblies made of specialty alloys. New non-destructive electronic property measurement techniques were investigated to assess the service life of time-dependent alloys, to determine the residual stress associated with welds and to assess the corrosion life of structures.

14. SUBJECT TERMS	15. NUMBER OF PAGES
Field Repair Weld, Welding Consumables, Aluminum and Magnesium Alloys, Electronic Property Measurement, Residual Stress	29
	16. PRICE CODE

17. SECURITY CLASSIFICATION OR REPORT	18. SECURITY CLASSIFICATION ON THIS PAGE	19. SECURITY CLASSIFICATION OF ABSTRACT	20. LIMITATION OF ABSTRACT
UNCLASSIFIED	UNCLASSIFIED	UNCLASSIFIED	UL

TABLE OF CONTENTS

1. INTRODUCTION

1.1. Development of Advanced Weld Repair Consumables and Welding Practices

1.1.1. Rapid Production of Welding Consumables for Repair of a Specific Alloy Composition
1.1.2. Development of Advanced Field Repair Welding Consumables for Light Metals (Al & Mg)

1.2. Development of Nondestructive Advanced Electronic Property Measurement Techniques for Repair-Weld Assessment

1.2.1. Correlation between Thermoelectric Power (TEP) Coefficient and Retained Austenite Content In Various Trip Steels
1.2.2. In Process Assessment of Weld Microstructure (Properties) to be Used as a Quality Control Practice
1.2.3. Use of Thermoelectric Property Measurement as a Method to Assess Residual Stress

2. SUMMARY OF THE IMPORTANT RESULTS

2.1. Advanced Weld Repair Consumable Development

2.1.1. Rapid Production of Welding Consumables for Repair of Specific Alloy Compositions
2.1.2. Develop Advanced Field Repair Welding Consumables for Light Weight Metals (Al and Mg)

2.2. Development of advanced Electronic Property Measurement Techniques for Repair-Weld Assessment

2.2.1. "In Process" Assessment of Weld Microstructure and Properties to be Used as a Quality Control Procedure
2.2.2. Use of Thermoelectric Property Measurement as a Method to Assess Residual stress in Nitrogen Strengthened (Non-Magnetic) Stainless Steel

3. ACCOMPLISHMENTS OF THIS RESEARCH CONTRACT PERIOD

4. COLLABORATIONS

5. LIST OF PUBLICATIONS FROM THIS RESEARCH CONTRACT PERIOD

6. LIST OF ALL PARTICIPATING SCIENTIFIC PERSONNEL

1. INTRODUCTION

The first issue is the development of advanced weld repair consumables and welding practices. The research of weld repair research was focused on repair in light metal assemblies being used to enhance the rapid deployment forces. The second issue involves the development of advanced nondestructive electronic property measurement techniques to nondestructively assess alloy phase content, microstructure, phase stability and alloy weld residual stress. The major emphasis of the assessment activities is the verification of the quality of the repair weld. In Section 1 of this report, an introduction and progress assessment for each project under the current ARO contract is given. Section 2 summarizes the important experimental results during this contract period. Section 3 details the accomplishments for each project.

1.1. Development of Advanced Weld Repair Consumables and Welding Practices

1.1.1. Rapid Production of Welding Consumables for Repair of a Specific Alloy Composition

The application of metal-cored wire welding techniques has led to substantial savings in terms of machinery-component replacement cost. Metal-cored welding consumables are cored wires made by forming a metal strip into a U-shape, which is then filled with fine metal powder of a specific elemental mixture. The powder filled strip is then formed to closure and drawn thru dies to make metal-filled cored welding wire. Current includes applications for metal-cored electrodes include the power generation industry, military equipment, and others. Until recently, metal-cored wire welding was restricted for many repair welding situations and was only acceptable for welding of structural steel applications. This limited use was due to a lack of inconsistency in weld metal composition [1].

A method to make small batches of maintenance metal-cored weld repair consumables in an efficient manner is being developed. Therefore, the composition of the weld deposit can be easily altered by changing the amount of metal powders added to the core of the welding wire.

The metal transfer efficiency of elements, such as Mn, Si, Ti, Cr, Ni, and C, across the arc was analyzed individually and then the interactions among the elements will be investigated. The elemental transfer efficiency needs to be established in order to modify the powder mixtures to allow for the achievement of accurately produced weld metal compositions. This practice is essential to repair specialty alloys used in some defense related equipment. The transfer efficiency of the elements depends on the interactions of the alloying elements, shielding gas, and mode of arc transfer (a function of Voltage and Current). Regression analysis was investigated to identify trends in the interactions of the different alloying elements.

The rapid production of custom metal-cored wire consumables for repair welding in the power-generating industry, military equipment, and other areas can be achieved in a shorter period of time and with reduced production cost when compared to a custom tailored solid wire welding consumable. It is essential to establish a thorough knowledge base to calculate proper powder mixtures, considering elemental loss, to achieve any specific weld composition. It is anticipated that a portable cored-wire making machine could be designed and become part of the integrated support machinery of a maintenance group.

During the present contract period the powder filling of the cored wire machine was designed and set up to be computer controlled (Figure 1). A data acquisition setup collects process variables to guarantee quality control. Numerous combinations of powder filled cored wires were made and welded.

In the production of metal-powder filled cored welding wires, the chemical consistency of the wire is crucial. The chemical consistency of the metal-cored wire depends on the homogeneous distribution of the elements in the metallic powders and uniform filling of the powders into the wire. The first problem is the segregation that might occur during the mixing of the different metal powders. To solve this problem and produce a homogeneous mixture, mechanical mixing in a blender (V-blender) was necessary before the metal powders were fed into the tubular sheath.

The other problem is that the uniform filling of the welding wire must be assured for the fabrication of the wires. A vibratory feeder gives a constant feeding rate, but different mixtures of powders result in different feeding rates. To solve this problem a data acquisition system was set up (a balance connected to a computer) to determine the feeding rate (grams of powder/unit of time) for each powder mixture. With the feeding rate of the powder known, the velocity of the wire drawing was adjusted to maintain a constant wire-filling ratio for all the possible wire chemistries formulated.

The project has received technical guidance from Mr. Joe Scott of Devasco Corporation, specialty welding wire producer. Devasco Corporation is prepared to make larger quantities of cored steel and aluminum experimental wires of smaller

diameter (0.035 and 0.045-in.) to be used in a portable GMA welding spool gun, which is becoming more common for field repair.

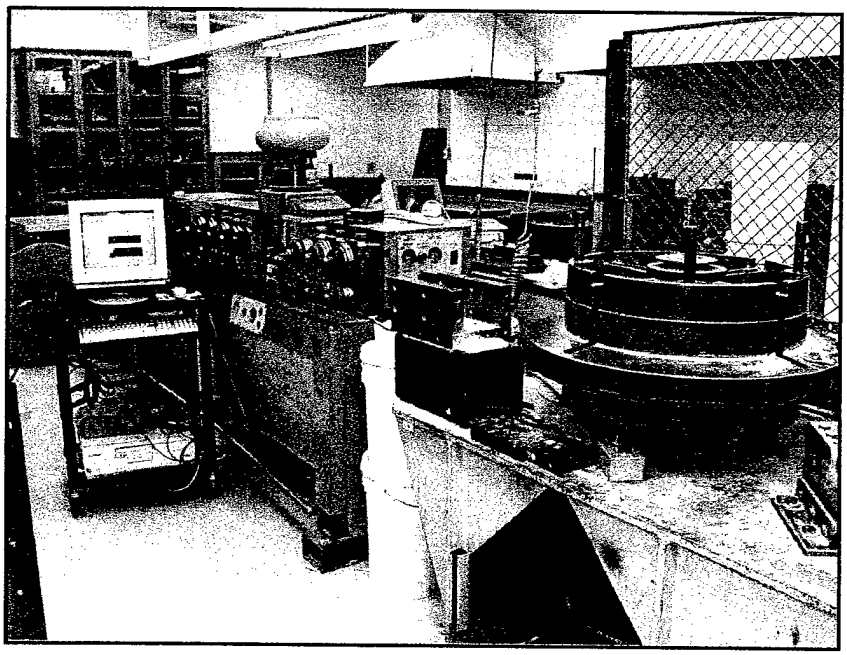

Figure 1 – Tubular wire mill and drawing stand used at CSM for fabrication of tubular wire with custom mixtures of core ingredients

1.1.2. Development of Advanced Field Repair Welding Consumables for Light Metals (Al & Mg)

Currently there is a push to make the U.S. defense forces more rapid and mobile through the use of light metals. Repair welding will be very important in maintaining the growing number of vehicles and structures using light metals. The most common of the structural light metals, aluminum, magnesium, and titanium are more difficult to weld than conventional structural steel [2]. Welding of light metals with current welding processes and consumables requires a high level of skill and process control to create acceptable welds, mainly to avoid hot cracking and porosity. These requirements present a problem when repair welding has to be conducted in less than ideal conditions.

Aluminum and magnesium alloys are attractive as materials for reducing the mass of the nation's defense force without compromising structural integrity. Magnesium's density is around 1.83 g/cm^3 for most of its alloys, which is about 2/3 the density of aluminum alloys. Both magnesium and aluminum alloys have good strength to weight ratios. Magnesium yields more readily, but it has a lower density value giving it a greater strength-to-weight ratio in comparison to aluminum. Both of the light metals are castable and weldable, however aluminum is much more formable due to its FCC crystal structure. Magnesium's hexagonal crystal structure limits its ductility. Both magnesium and aluminum have similar melting temperatures (648°C compared to 660°C for aluminum). During magnesium welding, less heat input is needed in comparison to aluminum due to its lower thermal conductivity. Based on the thermal conductivity and the material similarity in melting temperatures, it can be predicted that identical welding heat inputs will produce greater peak temperatures, wider and deeper welds, and slower cooling cycles in the magnesium [3]. Both aluminum and magnesium are welded with the same processes, such as GTAW, Laser welding, Friction stir welding, and others. In most cases welding needs to be performed in a controlled environment with well-controlled welding conditions. The welding of light alloys is not as forgiving as steel welding for many reasons, the most important of which is porosity problems. In order to successfully weld light alloys in the field, consumables need to be developed which will mitigate problems such as porosity and hot cracking, and provide shielding of weld metal in unpredictable environments.

The objective of this research was to develop easily weldable consumables that can be utilized in a lightweight and highly portable welding system. The most operator friendly manual welding processes are gas metal arc welding (GMAW) and flux cored arc welding (FCAW). Power supplies and wire feeding systems for these welding processes are generally

cumbersome and not highly portable. However, there is a portable welding spool gun on the market that is able to run off of automotive batteries. The Ready Welder, as it is called, is able to run on one, two, or three 12 Volts automotive batteries in series (military vehicles already operate on a 24 Volts electrical system) and can also be hooked up to a regular constant voltage power supply [4]. This portable spool gun can weld aluminum and steel using inert gas shielding, and can also be used for self-shielded steel welding. The Ready Welder with its cables and spools of wire fit within a case a little larger than a brief case. The 1 and 2-lb wire spools used with the spool gun are very common. Standard wire diameters of 0.035-in and 0.045-in can be used in the Ready Welder. The combination of a portable welding gun such as the Ready Welder and advanced welding consumables for light metals would allow rapid in-field repair by a moderately skilled welder. This research effort will develop flux-cored wires for the light alloys with a specific effort on wires with some degree of self-shielding that can be used in a portable spool gun welder.

1.1.2.1 Development of a Flux-Cored Aluminum Repair Consumable

ARO sponsored research has been undertaken at CSM to develop advanced flux-cored aluminum welding wire. Currently there is no commercial aluminum FCA welding wire on the market. There are a number of aluminum shielded metal arc welding (SMAW) consumables that can be purchased, however they are notoriously difficult to weld with and in most cases only produce marginal quality welds.

The study of fluxes for welding aluminum is not a new topic. A review of the literature shows that a variety of work has been conducted beginning in the early 1900's. However, despite past research the topic of fluxes for arc welding of aluminum still appears to be a vague and poorly understood area of welding science. Most of the work in the past appears to center on the use of salt systems incorporating fluoride and chloride compounds [5, 6, 7]. Salts are a common ingredient in brazing fluxes and are also used extensively in the refining and recycling of aluminum [8, 9, 10]. There are several characteristics of salt systems that make them attractive as an aluminum arc welding flux such as low density and low melting point. The binary salt systems of interest are NaCl-KCl, NaF-NaCl, KF-KCl, and NaF-KCl [8]. The use of fluorides is attractive due to the fact that fluorine has a high affinity for hydrogen and fluoride based fluxes also can incorporate large amounts of absorbed oxygen. Hydrogen is a major cause of porosity in aluminum welds. Other compounds such as Cryolite (Na_3AlF_6) can help with the wetting of the weld because of its good solubility of aluminum oxide. However, salts make a welding arc extremely unstable and due to the high arc temperatures harmful compounds can be generated.

Due to the inherent difficulty with making small diameter cored wires for each flux composition, all of the preliminary welding was done with a submerged arc welding process. All studies were carried out using 6061 aluminum base plate and 4043 aluminum filler wire due to the fact that this combination is widely used. After trying a variety of salt flux combinations, the weld quality and the weld environment were determined to be unacceptable for several reasons, the first of which is the harmful fluoride and chloride fumes given off during welding. These fumes do pose a health hazard and are corrosive. In addition, there are problems with excessive moisture absorption and arc instability. Severe arc stability problems in addition to extremely poor weld quality were found during testing of several binary systems. Shelf life of a cored wire is another possible issue because some salts can corrode the aluminum sheath over time. In addition, salts were found to absorb moisture, which can cause hydrogen porosity in aluminum welds

1.1.2.2. Welding Assessment of Magnesium-Lithium Alloys

Currently, the weldability of the two light-weight magnesium-lithium (Mg-Li) alloys are also being investigated. Magnesium with over 10-wt. pct. lithium alloy addition exhibits a BCC crystal structure [11]. This situation often offers a significant improvement in formability when compared to HCP magnesium alloys. Magnesium is commonly used as a casting alloy. However, a magnesium alloy with acceptable weldability and improved formability offers an economical advantage by allowing the use of formed wrought material along with acceptable welding procedures to fabricate welded technical assemblies [12].
In this research the weld microstructure and properties are being characterized for two magnesium-lithium alloys. The first alloy contains 7.5-wt. pct. lithium making it an $\alpha+\beta$ alloy. The other alloy contains 10.2-wt. pct. lithium making it a fully bcc (α) alloy. Autogenous GTA welds have been made on both Mg-Li alloys in addition to a traditional magnesium alloy. A large glove box with a purified and recirculating argon environment was constructed for welding Mg-Li and other reactive metals (Figure 2). The microstructures are being identified, characterized, and compared in regard to weldability.

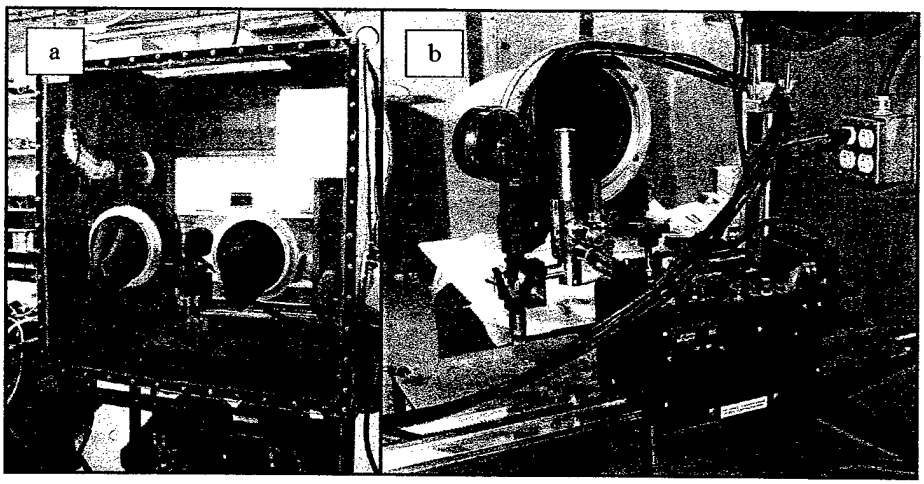

Figure 2. a) Front View of inert gas environment welding glove box which was set up for welding of Mg-Li and other reactive metals b) A picture of the inside of the glove box showing the motorized torch carrier with a GMAW spool gun attached. The box is wired to allow the use of GMA and GTA welding.

Photomicrographs of weld cross-sections from both Mg-Li alloys show welds that are extremely wide with very shallow penetration (Figure 3), much more so then in an aluminum weld with the same parameters. The wide and shallow bead is most likely the result of several factors. One factor being the fact that magnesium has a lower thermal conductivity than aluminum and the second is surface tension driven flow (Marangoni flow) of the weld pool. The surface tension driven flow is most likely the cause of the extremely shallow penetration and wide weld bead. It is known that the surface tension of magnesium drops as temperature increases resulting in the outward flow of molten metal from the center of the weld pool. This outward flow of molten metal minimizes the penetration and maximizes the width (Figure 4a). In contrast if the flow of molten metal in the weld pool were to reverse, flowing from the edge of the weld pool to the center, the penetration of the weld would be maximized and the width minimized (Figure 4b). The Marangoni flow of the Mg-Li weld pool presets a hurdle that will need to be overcome in order to make this alloy more weldable.

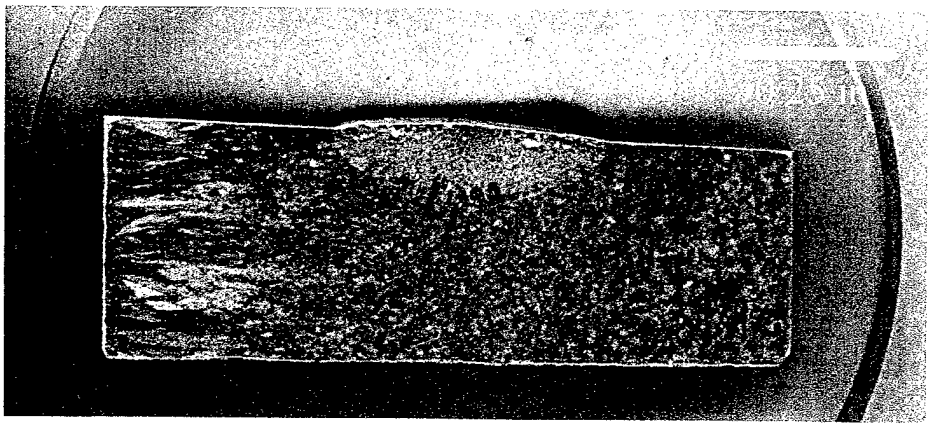

Figure 3 – Cross section of a GTA autogenous weld on magnesium-lithium (7.5 wt. pct. lithium) alloy. Note the shallow penetration and large width.

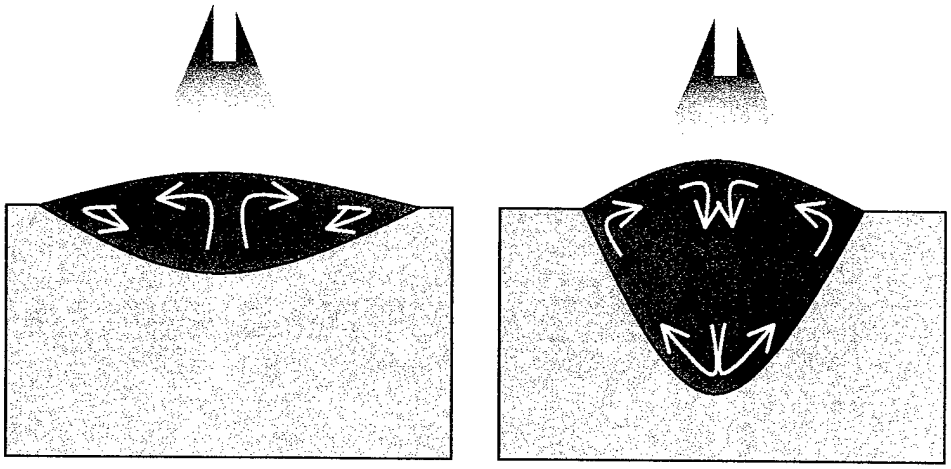

Figure 4 - Schematic figures depicting how molten weld metal flow effects the weld depth and width. a) Materials such as magnesium, which have a surface tension that decreases with temperature, are prone to surface tension driven flow (Marangoni flow) which causes shallow and wide weld beads. b) When the molten metal flow is reversed the resulting weld beads generally have deeper penetration.

1.1.2.3. Development of a Titanium Flux-Cored Consumable

Another faculty researcher within the Center for Welding, Joining and Coating at CSM, Professor Stephen Liu, is currently working on a flux-cored titanium consumable. This project bears some resemblance to the work being done with the flux-cored aluminum research that is proposed here. The flux-cored titanium research is not part of the work presented here, however, close contact is maintained with Professor Liu regarding approaches being investigated for the development of the titanium self- shielded welding consumable in order to expedite the aluminum consumable project.

1.2. Development of Nondestructive Advanced Electronic Property Measurement Techniques for Repair-Weld Assessment

Three research initiatives are currently being pursued under the general category of advanced electronic property measurement techniques for weld assessment. All three projects are investigating the use of Thermoelectric Power (TEP), i.e. the Seebeck effect, for assessment of weld microstructure, phase content, and residual stress. Section 1.2 gives an introduction, background, and progress report for each of the three projects. These advanced electronic property measurements are made in the CSM facility equipped by an ARO DURIP equipment grant.

1.2.1. Correlation Between Thermoelectric Power (TEP) Coefficient and Retained Austenite Content in Various TRIP Steels

The presence of retained austenite in the hardened steel microstructure generally induces significant changes in certain mechanical, engineering, and processing properties of steels. Techniques allowing accurate measurements of the retained austenite, as well as methods for its control during processing have grown in importance for the quality control of weld defense related structures and assemblies. Also, Kimura *et al.* [13] observed that the content of retained austenite is a critical factor in the corrosion of structural steels. Because the volume of retained austenite is affected by thermal experience of welds, accurate measurement of retained austenite content was required to minimize the sulfide stress cracking.

Also, retained austenite is known as an intermediate hydrogen trap, which results in hydrogen release in the presence of plastic strain and low temperatures [14]. The control of retained austenite and trapped hydrogen can decrease hydrogen-

cracking susceptibility in weld metal of high strength steels. Therefore, a fast and nondestructive measurement of retained austenite content is essential to prevent hydrogen assisted cracking in high strength steel weldments.

Many different techniques for the measurement of retained austenite in martensite have been applied and developed in the last thirty-five years. However, an accurate measurement of retained austenite has always been challenging when retained austenite contents are at very low levels. Quantitative optical microscopy has generally been satisfactory as long as the retained austenite content is higher than 15 vol. pct. [15]. With less than 15 vol pct., difficulties develop during etching and from resolution limitation. A more accurate retained austenite measurement technique is X-ray diffraction method. The detailed methods of these X-ray diffraction and optical microscopy techniques can be found in several papers [16, 17]. However, both techniques show quite a bit of divergence in the reported values depending on measurement technique and method of calculations.

The TEP measurements of steel specimens containing retained austenite TRIP were conducted at CSM because of a relatively large quantity of retained austenite contents. Retained austenite in TRIP steel has been used to relieve the stress during deformation and to achieve a high work hardening rate from transformed martensite at the end of deformation. Therefore, optimum content of retained austenite is a requirement and differs depending on different applications, which makes accurate measurement of retained austenite even more critical.

The results of TEP coefficient as a function of retained austenite content are shown in Figure 5. The results indicate that the TEP coefficient corresponds well to volume percent of retained austenite. However, a few data points did not correlate to the linear regression line. The test results from ECO 5W and 6W specimens, which were oil quenched directly following the intercritical annealing process, were lower than the linear regression line. The observations suggest that microstructural changes occurring during the quenching process may have affected the final value of the TEP coefficient, because the quenching process for intercritically annealed specimens result in a martensitic transformation for the final microstructure. Also, this martensitic transformation can generate dislocations due to transformations with shear mechanisms. Generation of dislocations may affect the TEP coefficient of final microstructure.

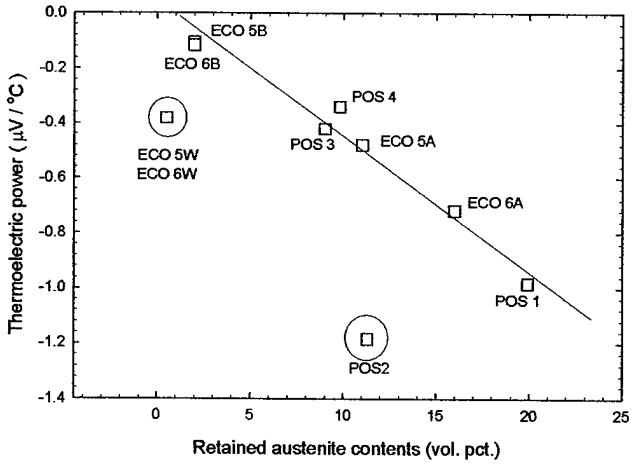

Figure 5 - The measured TEP coefficients as a function of retained austenite content for TRIP steel specimens obtained from POSCO Company. The data points in the solid circle represent values deviating from linear correlations. ECO 5W and 6W are oil quenched right after the intercritical annealing process.

To further demonstrate the capability to assess retained austenite content with the TEP surface contact measurement, the retained austenite content was gradually changed by varying the time in an isothermal transformation process. When TRIP steel is isothermally held at a temperature of 450°C, austenite transforms to bainite. In scanning electron micrographs retained austenite appears smooth and has a featureless shape, leading to easy distinction from ferrite and bainite. However, there are no observable structural differences between ferrite and austenite. Actual retained austenite measurements were conducted with X-ray diffraction analysis. By changing transformation time from 1 to 15 minutes, the retained austenite contents were varied from 12 to 1 vol. pct., as shown in Figure 6. The changes in the TEP coefficient with different amounts of retained austenite content are shown in Figure 7. The measured TEP coefficient correlates well with the retained austenite content, and practices could be established to increase quality of TRIP steels. These results illustrate the new electronic metallographic practices for rapid microstructural characterization. Here a nondestructive testing procedure involving two electronic surface contact probes can determine, when calibrated to a standard, the

amount of phase or even microstructure present. This practice can be performed easily in the field and can support weld repair operations.

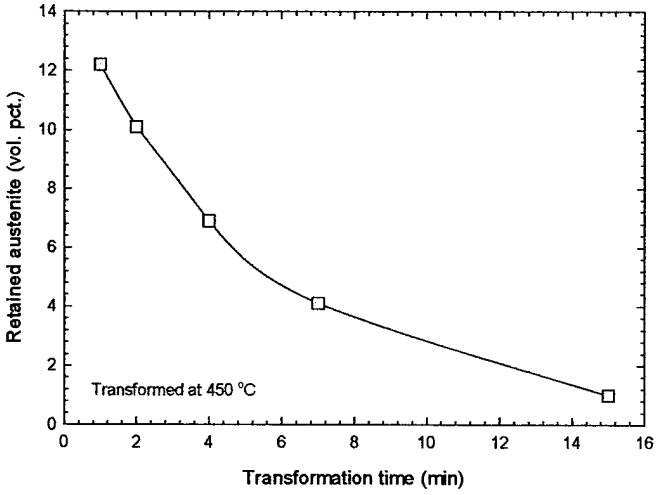

Figure 6 - Changes in retained austenite content (obtained by XRD) for TRIP steel as a function of isothermal transformation time at 450 °C.

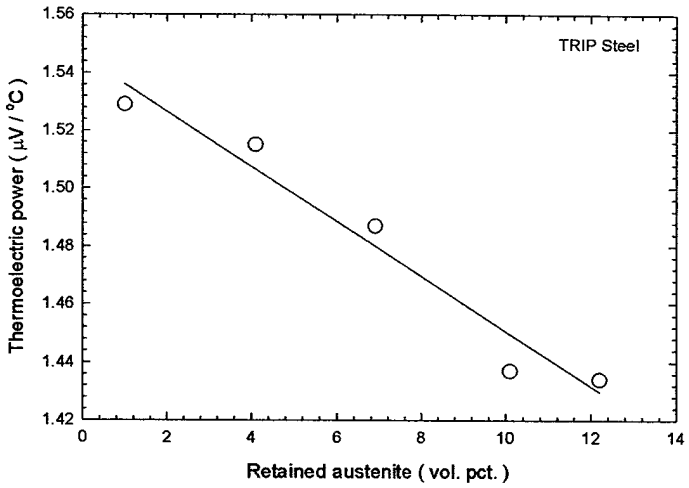

Figure 7 - The measured TEP coefficient as a function of retained austenite content for heat treated TRIP steels (CSM1-CSM5).

1.2.2. In Process Assessment of Weld Microstructure (Properties) to be Used as a Quality Control Practice

Weld microstructure evaluation during the welding process has been challenging due to its technical difficulties. However, quality control of final weld microstructure needs simple, accurate, and nondestructive measurement methods for field uses. Advanced electronic property measurement, such as thermoelectric power (TEP) and magnetic measurements, can be used effectively as a new quality control tool for repair welds. Schematic drawing of Thermoelectric nondestructive testing, based on contact with the just deposited weld metal during cooling, is shown in Figure 8. Because TEP measurement is very sensitive to different microstructures, any microstructural changes occurring during cooling should be detected using this technique.

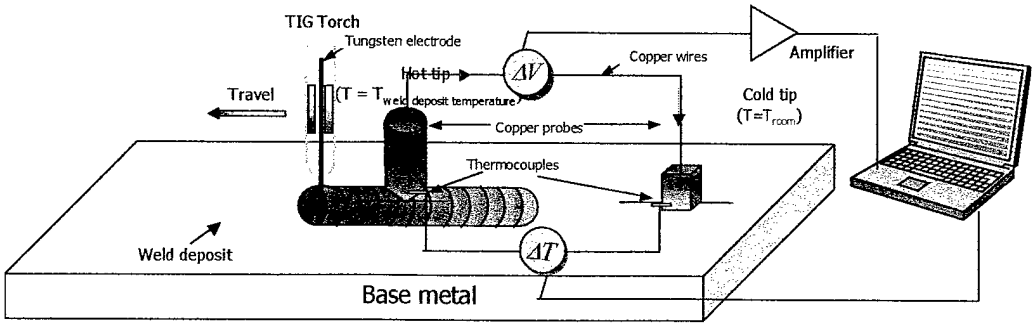

Figure 8 - Schematic setup used for TEP measurement on cooling directly after weld solidification.

A given weld microstructure is dependant on the specific weld thermal experience; that is heat input as well as heat extraction (plate thickness), and thus should have its own characteristic TEP signal profile. If the TEP signal profile is outside of a determined acceptable profile then changes must be made to the welding parameters to generate the required weld microstructure and properties for repair-welds.

When this nondestructive electronic property measurement practice is developed and calibrated it offers the ability to make process control decisions at the time of welding or material fabrication. The measurement of indications, such as time periods, and temperatures of weld phase transformations produces a sufficient signature that can be correlated to a resulting microstructure. The weld microstructure can than be correlated directly to weld properties. Thee collected electronic signal offers an easy way for data acquisition so that the microstructural evolution of each weld can be electronically stored. The TEP testing equipment and arrangement can be packaged to be useful for field weld repair.

1.2.3. Use of Thermoelectric Property Measurement as a Method to Assess Residual Stress and Nitrogen Content in Nitrogen Strengthened (Non-Magnetic) Stainless Steel

The research work characterized the effect of nitrogen in austenitic stainless steel (non-magnetic) weldments and residual stress utilizing thermoelectric power. It is necessary to assess the residual stresses resulting from weld solidification shrinkage, however there are other factors that can also contribute to weld residual stress. For example, the addition of interstitial nitrogen to austenitic stainless steel results in measurable lattice strain. Dependent upon the solubility of nitrogen, there may be formed nitrides as well as nitrogen in solution in the austenite matrix. So, it is important to decipher and quantify the strain effects resulting from nitrogen in solution, formed nitrides, and residual stresses from welding.

Nitrogen-strengthened austenitic stainless steel (non-magnetic) samples are nitrided to different nitrogen concentrations. The nitrided samples then was put into a Gleeble thermomechanical simulator, for simulation of a weld-heat affected zone, 1 mm from the fusion line without inducing weld residual stresses. The purpose of the Gleeble simulation is to be able to assess the change in the nitrogen concentration due to the thermal experience and to measure the change in the Seebeck coefficient before and after the thermal experience. The thermal experience may cause the nitrogen to form nitrides, thus changing the amount of induced lattice strain and altering the beneficial affects of nitrogen as an interstitial strengthener. The Gleeble allows a simulation of the weld-heat affected zone without the residual stress from solidification shrinkage, which allows the determination of the separation of the affects of both residual stress and nitrogen on the Seebeck coeffcient. The samples are analyzed using electron microscopy and micro-kjeldahl titration method to measure the nitrogen in solution and nitrogen in the form of nitrides. The Seebeck coefficient is measured at three different points: before nitriding, after nitriding, and after Gleeble simulation. The Seebeck coefficients from these samples are be compared to the Seebeck coefficient in the heat-affected zone of an actual welded nitrided sample. This investigation provides useful information for the assessment of the relative contributions of these two effects, residual stress and nitrogen, in nitrogen-strengthened stainless steel welds.

2. SUMMARY OF THE IMPORTANT RESULTS

2.1. Advanced Weld Repair Consumable Development

2.1.1. Rapid Production of Welding Consumables for Repair of Specific Alloy Compositions

2.1.1.1. Fabrication of strip to metal powder filled cored welding wires for rapid production of small batches

During the this contract period specialty metal-cored wires were made to meet the compositional requirements of at least three example defense related alloys for repair welds. These wires were used to weld specialty alloys to evaluate the ability to achieve a specific weld composition. The welds were analyzed for composition, and microstructure were evaluated as to whether they come within the acceptable composition range for the specialty alloys. The performance of the welding consumable during welding was also evaluated for arc stability, bead morphology, weld bead defect concentration, and ease of handling. This evaluation used "figure of merit" for each weld requirement. Also, the welding process will be evaluated for arc stability, elemental transfer efficiency, and the metal transfer mode.

First, the transfer efficiency of elements across the welding arc has been investigated to obtain accurate transfer efficiencies needed for programming the proper powder additions to the cored steel wire. This computer control setup allows rapid production of cored steel wire by introducing the correct powder fillings into the cored steel wire to produce weld repair consumables requiring a specific composition. The cored wire approach become advantageous when existing solid welding wires was not available for compositional requirements. Two matrixes of experimental wires were designed to determine the coefficient of transfer efficiency. Knowing the transfer coefficients and the composition of the steel-cored wire and welding parameters can be selected to achieve the required chemical composition of the deposited weld metal. The transfer efficiency of the elements is dependent upon the interactions of the alloying elements, the shielding gas, and the mode of metal transfer across the welding arc.

The design of welding consumables is a complex task because there is not a perfect mathematical-metallurgical model that can predict the relationship between the chemical composition of the weld deposit and the chemical composition of the welding wire consumables. Therefore, techniques such as regression analysis and neural networks are going to be applied in this investigation to accomplish this task.

Two studies were completed to look at the transfer efficiency of elements across the welding arc. The first study was designed to evaluate the transfer of individual elements across the arc. As shown by the matrix in Table 1, a series of 25 wires are being fabricated to test the transfer of individual elements.

Table 1. Experimental matrix for testing of single element transfer across a welding arc.

FeMn	FeTi	FeSi	FeCr	Ni
100%	100%	100%	100%	100%
80%	80%	80%	80%	80%
60%	60%	60%	60%	60%
40%	40%	40%	40%	40%
20%	20%	20%	20%	20%

(Percentages with respect to the total powdered metal in core – remainder of core material is iron powder)

The second study was designed to examine the interactions between Mn, Ti, Si, Cr, and Ni when all five elements are combined in a metal cored welding wire. A statistical experimental design approach is used to reduce the number of necessary experimental cored wires. A program called Design-Expert 6 is used to create an experimental matrix. For each element (C, Mn, Si, Ti, Cr, Ni), a minimum and maximum powder content is chosen. For this investigation the program determined that a total of 38 experiments are needed to characterize the transfer efficiencies.

The transfer efficiency of each element was analyzed in the presence of three different mixtures of gases: Ar-2%O_2, Ar-1%O_2 and CO_2. For each of these gases a transfer mode map (spray, globular, and short-circuit) on a volt-ampere plot was made to define the welding parameters, such as voltage and wire feed rate, that were to be used for each experimental wire. Multi-pass welding was used to avoid the influence of the base plate in the recovery of the alloying elements. The subsequent chemical analysis of the weldments are under investigation with an emission spectrometer.

After all the data were collected, the analysis of the multiple responses (recovery of the different elements) was carried out to choose the appropriate model. The optimization of one response or the simultaneous optimization of multiple responses was performed graphically or numerically using the program Design-Expert 6.

2.1.1.2. Selection of welding parameters

A DAQ (Data Acquisition System) was connected to the welding machine to acquire the voltage signal during the welding of the experimental wires. The frequency of acquisition used for voltage signal was 10 KHz. The signal acquired (voltage signal) for the welding of the experimental wires were analyzed to choose appropriate welding parameter to be used. The idea was to find the appropriate parameters that can provide clear spray, transition and short-circuiting transfer mode for all the wires. Each wire was tehn tested at the selected parameters. A computer program was written to identify the peak-valley voltage difference for each voltage-time trace and to calculate the peak-voltage difference to acquire dV for each transfer event. This program was designed to identify transfer mode in which weldment was made. The program was written in the Mat Lab Software.

The criteria used to distinguish the transfer modes is the following:

hort-circuit	S dV > 8 volts
Globular	1 < dV < 8 volts
Spray	0.5 < dV < 1 volts
Noise	dV< 0.5 volts

Some examples of the voltage signals that were analyzed are presented for wires with 80%FeMn and 1%O_2 are shown in Figure 9.

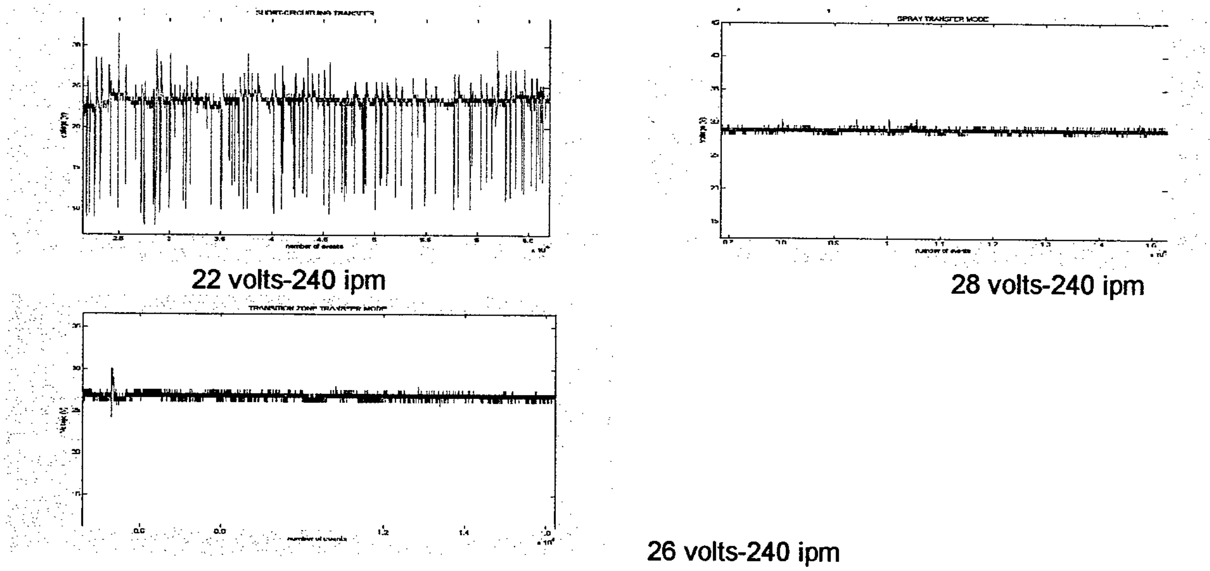

Figure 9. Examples of the voltage signals for wires with 80%FeMn and 1%O_2

2.1.1.3. Metal Transfer Mode Map

The consumable wire used to create the metal transfer mode map was a 100%-FeMn (30% filling ratio- diameter: 0.055 inch) and the shielding gas Ar-1% O_2. All the arc voltage signals from the experimental weldments were examined using the dV for metal transfer mode determination. By identifying the individual droplet transfer event from the arc voltage traces, the relative percentage of each transfer mode, that is, number of transfer events of a particular mode divided by the total number of transfer events, was calculated. With this information a metal transfer mode map was determined.

There are two important considerations for the use of this method. First, no single transfer mode is observed. On the contrary, two or more transfer modes coexisted at all times. Second, the presence of globular and/or short-circuiting transfer events, even in a small number can affect the arc voltage signal fluctuations significantly. Thus, a mixed transfer with over 10 percent globular on a spray background can be classified as a predominately globular transfer. Mixed modes with over 3 percent short-circuiting can be classified as a predominately short-circuiting.

The map of metal transfer mode in different wire feed rate is shown in the figure 10 . This map was taken as a model for the rest of the wires, expecting that the metal transfer mode did not change when the wire changed. The lack of change in the transfer mode was confirmed later when the multipass weldment were made with wires of different compositions.

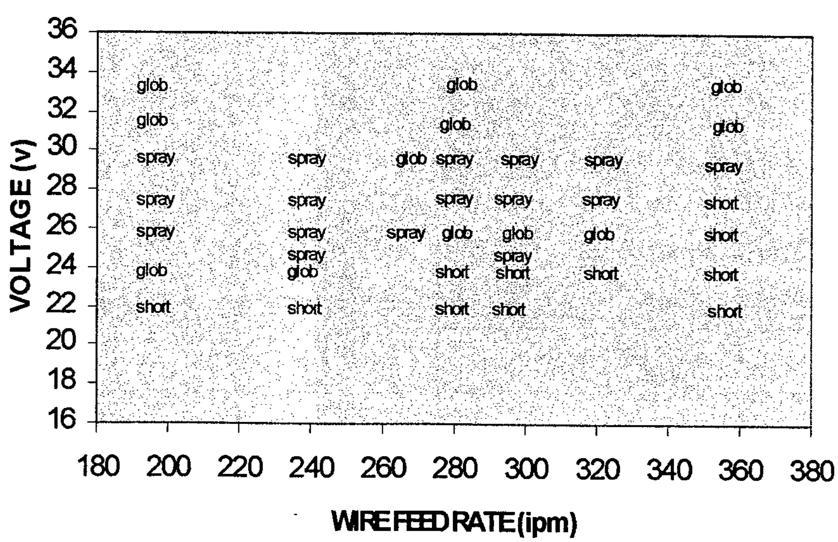

Figure 10. The map of metal transfer mode of 100%-FeMn (30% filling ratio- diameter: 0.055 inch) and the shielding gas Ar-1% O_2

2.1.1.4. Metal Transfer Mode Map Welding of samples

For each experimental metal-cored wire, fourteen multipass weldment were made of which six were made using Ar-1%O_2 as shielding gas, six were made using Ar-2%O_2 ,and two with CO_2.

A total of 350 multipass weldments were made for this investigation. A copper dam was used to make the multipass weldment. The dam helped to make the welding of one layer on the top of the next of the multipass weldment much easier than a typical multipass weldment. Low carbon steel plates were used as base plate for the multipass weldments (one-inch thick). These passes were made one on top of the other. There three pass weldments and this typical dimensions are shown in Figure 11 and 12, respectively.

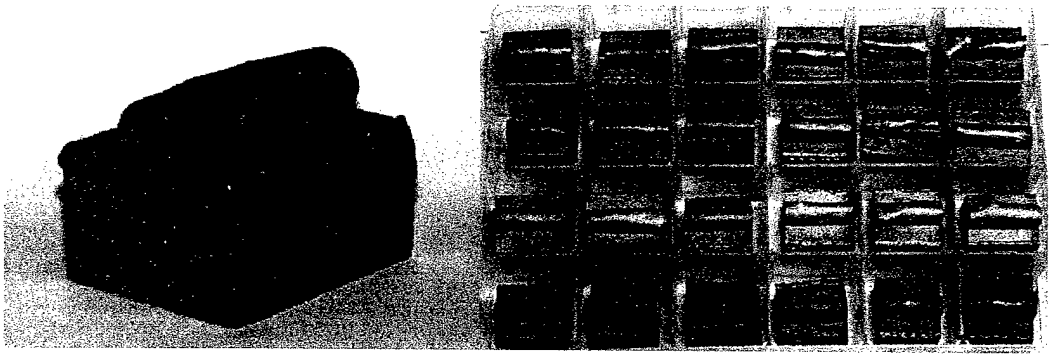

Fig. 11. Pictures of three-pass weldment

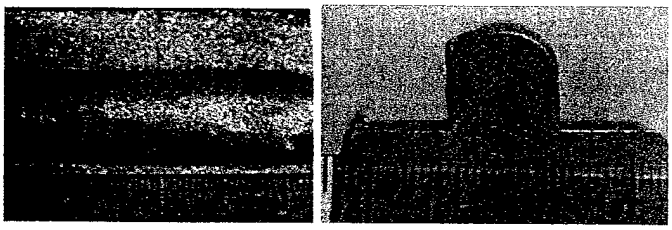

Fig. 12. Dimensions of a typical weldment

2.1.1.5. Chemical Analysis of the wires and weldments

The chemical analysis of the experimental wires was necessary in order to calculate the metal transfer efficiency of each element. Inductively Coupled Plasma (ICP) Spectroscopy is the chemical method chosen for this analysis. This process involves the digestion of the wire, to put the elements in solution. Then, this solution can be inserted in the ICP equipment for the analysis.

The elemental content of the wires are:

FeSi cored-wires	wt. pct Si-max: 14.4	wt. pct Si-min: 2.9
FeMn cored-wires:	wt. pct Mn-max: 19.5	wt. pct Mn-min: 3.9
FeTi cored-wires:	wt. pct Ti-max: 12	wt. pct Ti-min: 2.4
FeCr cored-wires	wt. pct Cr-max: 14.8	wt. pct Cr-min: 3
Ni cored-wires:	wt. pct Ni-max: 30	wt. pct Ni-min: 6

These minimaum and maximum element values are theoretical chemical content of the wires, calculated based on the filling ratio of the wire and the chemical composition of the powder ingredients. The chemical analysis of the weldments was made in a Glow Discharge Spectrometer. This equipment was chosen because of the simple and easy sample preparation, which involves just the preparation of a clean and flat surface top of the weldment with an aluminum oxide abrasive paper.

2.1.2. Development of Flux Cored Aluminum Welding Consumables

Two self-shielding methods for aluminum welding have been investigated. In the first method various salt-based fluxes, which are traditionally used for aluminum SMAW, were investigated using a submerged arc process. In contrast a more novel technique for self-shielding by storing inert gas in zeolite powders, which can be placed in a cored wire, was explored. Experiments were conducted to determine storage capacity of several zeolite powders.

Currently there is no aluminum FCAW wire on the market. There are a number of aluminum SMAW consumables available, but they are notoriously difficult to weld and in most cases only produce marginal quality welds. Despite past research the topic of fluxes for arc welding of aluminum still appears to be a vague and poorly understood area of welding science. Most of the work in the past appears to center on the use of salt systems incorporating fluoride and chloride compounds. Salts are a common ingredient in brazing fluxes and are also used extensively in the refining and recycling of aluminum. There are several characteristics of salt systems that make them attractive as an aluminum arc welding flux such as low density and low melting point. The binary salt systems of interest were NaCl-KCl, NaF-NaCl, KF-KCl, and NaF-KCl. The use of fluorides is attractive due to the fact that fluorine has a high affinity for hydrogen, and fluoride based fluxes also can incorporate large amounts of absorbed hydrogen which is a major cause of porosity in aluminum welds. Other compounds such as Cryolite (Na_3AlF_6) can help with the wetting of the weld because of its good solubility of aluminum oxide. However, salts make a welding arc extremely unstable and due to the high arc temperatures harmful compounds can be generated.

Due to the inherent difficulty with making small diameter cored wires for each flux composition, all of the welding was done with a submerged arc welding process. All studies were carried out using 6061 aluminum base plate and 4043 aluminum filler wire due to the fact that this combination is widely used. After trying a variety of salt flux combinations, the weld quality and the weld environment were determined to be unacceptable for several reasons, the first of which is the harmful fluoride and chloride fumes given off during welding. These fumes do pose a health hazard and are corrosive. In addition, there are problems with excessive moisture absorption and arc instability. Severe arc stability problems in addition to extremely poor weld quality were found during testing of several binary systems. Shelf life of a cored wire is another possible issue since some salts could corrode the aluminum sheath over time. In addition, salts were found to absorb moisture which can cause hydrogen porosity in aluminum welds. Due to all the aforementioned issues the decision was made to pursue other methods of shielding for aluminum welding.

The concerns of using salts as fluxing agents for aluminum welding prompted a search for a safer method of shielding. Hence, a method of storing argon in the core of a welding wire was undertaken. Nanoporous solids were identified as possible candidates for argon storge. Zeolites, which are nanoporous aluminosilicates (0.3-2.0 nm pore diameter), were investigated to determine their ability to store the argon gas. Zeolites, which are commonly used as molecular sieves, have a highly porous structure (up to 50 % or total volume). While zeolites do not normally absorb inert gasses such as argon investigations were carried out to determine if a fine zeolite powder could be forcefully charged with the gas. A variety of tests were performed on two types of zeolite powders (grade 3A and 4A) to if argon can be stored. The charging procedure was conducted at high pressure (200 psig) and temperature (250°C) followed by cooling with liquid nitrogen. The powder was then returned to room temperature and the pressure released. Thermo-gravimetric testing (STA analysis) of the charged powders found that no argon was retained in the zeolite powder at room temperature and pressure. A method of sealing the powder such as a glass Sol-Gel coating is suggested to aid in retaining argon in the powder.

Investigation into salt fluxes for aluminum welding found that the risks involved necessitated research of alternate weld shielding methods. Therefore a novel approach of using a porous zeolite powder to store inert gas was investigated. Unfortunately, it was found that zeolite powder will not retain argon at room temperature and pressure. A method of encapsulating the nanoporous zeolite powders to retain argon is suggested for future study.

2.1.3. Weldability Investigation of Magnesium-Lithium Alloys

All metallurgical examinations of the as-cast base materials revealed that the microstructure of the 7.5-wt.pct. lithium alloy differ significantly from its lithium-rich counterpart. Unlike the 10.2-wt.pct lithium alloy, the 7.5-wt.pct. lithium alloy exhibited a dual microstructure of the α and β phases. On Figure 13, which is an optical micrograph of the two-phase alloy in its as-cast condition, the brighter micro-constituent was identified as the α-Mg phase and the darker micro-constituent as the β - Mg (β-Li) phase. Microscopic examination of ingot cross-sections in Figure 14 revealed the typical eutectic microstructure of the 7.5 wt. pct. Li alloy, except in the ingot periphery where columnar growth clearly occurred from the mold walls.

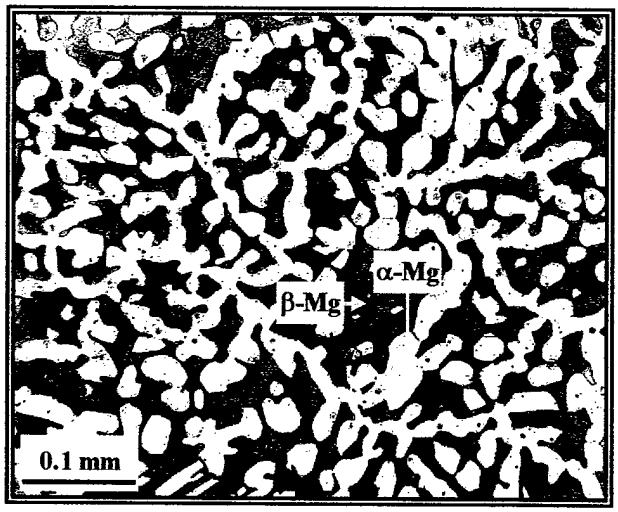

Figure 13. Optical micrograph of the as-cast 7.5-wt.pct. lithium alloy.

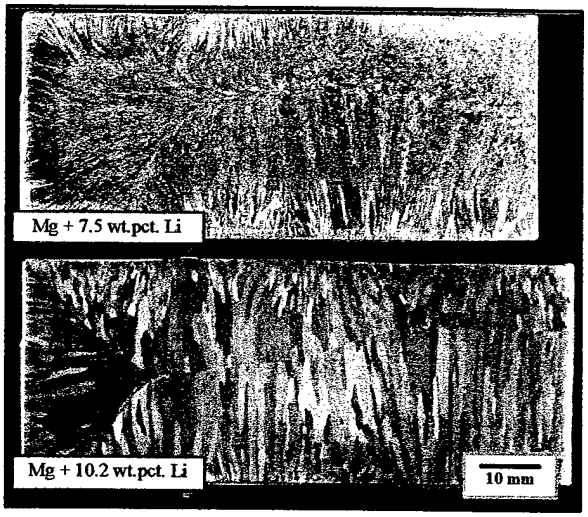

Figure 14. As-cast grain structure of the two lab-made magnesium-lithium billets (5-pct. nitric acid etch).

In stark contrast with the 7.5-wt.pct. lithium alloy, the 10.2-wt.pct. lithium alloy did not exhibit a dendritic microstructure, but instead, large equiaxed grains which are well depicted in Figure 15. Like in the dual-phase 7.5-wt.pct lithium alloy, long columnar grains were detected on the ingot periphery (Figure 14). The absence of any noticeable solute partitioning between the liquid and solid phases, as pointed out by the binary phase diagram, well explains the possibility that constitutional undercooling was not available. Lack of constitutional undercooling perfectly substantiates the grain structure seen in the single-phase alloy(Fig 15).

Figure 16 depicts typical bead-on-plate welds in the two alloys. Repeated cross-sectional measurements in random locations confirmed that the weld beads were comparable in width and depth of penetrations in both alloys. The shallow penetration seen in these wide weld beads indicates that heat extraction by conduction away from the liquid pool was particularly effective. Lack of penetration was certainly not promoted by the material's thick gage, which established three-dimensional heat flow conditions.

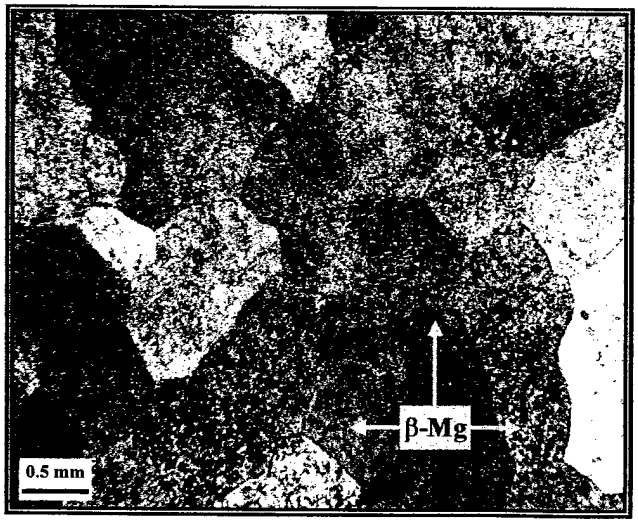

Figure 15. Optical micrograph of the as-cast 10.2-wt.pct. lithium alloy (polarized light)

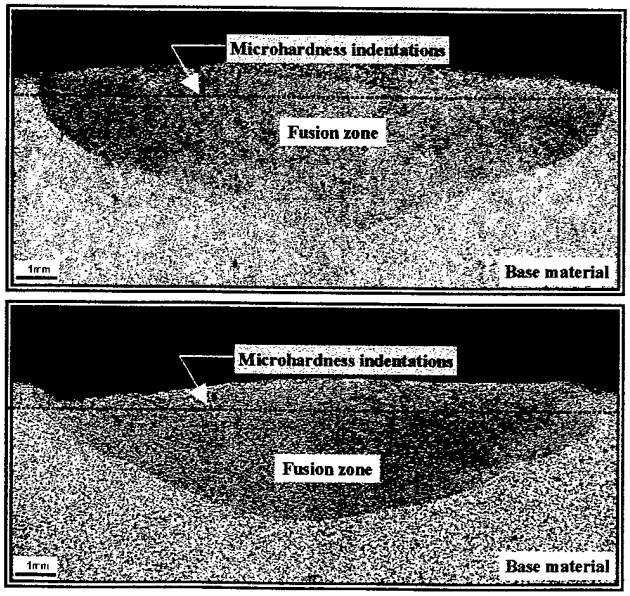

Figure 16. Optical macrographs of weld cross-sections in the 7.5-wt. pct. lithium (top picture) and the 10.2- wt. pct. lithium (bottom picture)

Marangoni, or surface-tension-driven flow can also be invoked to discuss the lack of weld penetration seen in Figure 5. Marangoni flow is usually predominant at low welding currents where the Lorenz electromagnetic force is comparatively

small, and in materials where surface tension decreases with temperature, as with all pure substances and most alloys. For the welding of thin gages, Marangoni flow is normally of little concern, except that it may occasionally create welds of uneven widths, which may result in various degrees of underbeads. Limited weld penetration is however an issue to overcome with thick gages or in the repair welding of castings. Based upon Figure 16, lithium has clearly a negligible effect on either the thermal physical properties, or in reversing the Marangoni flow during welding. To improve weld penetration, future work may be needed to identify alloying elements that will affect surface tension over the pool, either by being surface-active, or by simply decreasing the rate at which alloy surface tension decreases with temperature.

In the two alloys of this study, weld heat affected zones were not observed, which could have been expected. First, the as-cast base material is in a quasi-equilibrium condition, as opposed to a metastable state resulting from cold-rolling or precipitation-strengthening, which would provide enough driving force for subsequent microstructural transformations upon reheating. In cold-worked or strain-hardened materials, recrystalization and grain growth typically occur. In precipitation-strengthened alloys, overaging cause coarsening of precipitates that loose coherency.

For the 7.5-wt.pct. lithium alloy, Figure 6 compares microstructures before and after welding. It is seen that the $\alpha+\beta$ eutectic microstructure developed after welding is considerably finer, as could be expected from the faster cooling induced by the traveling heat source. In Figure 6, the lighter and more predominant structure is the α-Mg phase and the darker phase is the lithium-richer β -Mg (β-Li) phase. The weld microstructure seen in Figure 7 is typical of the center of the weld where a fine lamellar α Mg phase, dispersed in the β-matrix can be observed.

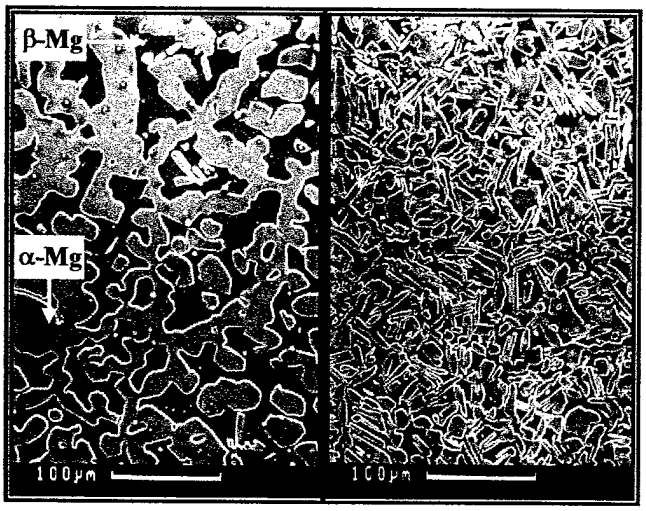

Figure 17. Secondary electron images comparing base material (left) and weld metal (right) microstructures in the 7.5-wt.pct. lithium alloy

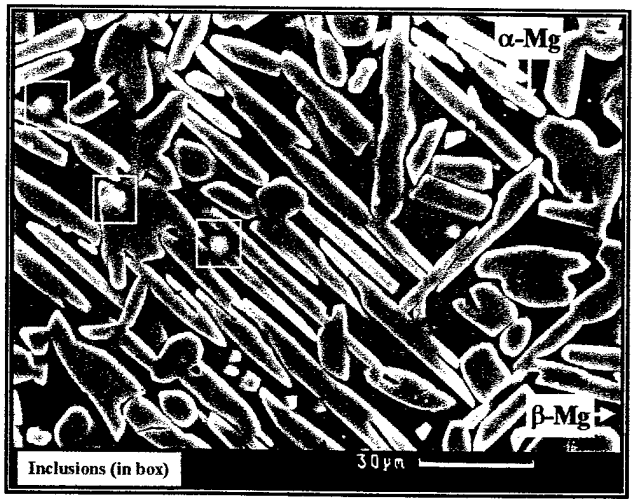

Figure 18. SEM image of the fusion zone in an autogenous GTA weld made in the 7.5-wt.pct. lithium alloy

Figure 18 presents a high-magnification secondary electron image showing an unusual solidification microstructure. Many of the α-phase lamellas appeared to have grown parallel to each other, if not impeded in their growth by other intersecting lamellas. Such phase morphology, characterized by high aspect ratios, indicates that crystal growth was faster in certain crystallographic orientations (probably closed-packed directions) and that interfacial tension between the two phases must be comparable, as pointed out by the flat interfaces. Improved toughness caused by crack deflections at internal boundaries may be an advantage offered by this new phase morphology. Detailed properties of the individual phases seen in Figure 18 may therefore be considered for future studies. In Figure 18, small spherical particles can also be detected. They are most likely oxide inclusions, produced as a result of the high reactivity of these alloys. Oxides may have been introduced either during melting (either casting or welding) or during polishing with alumina and silica.

Figure 19, which depicts microstructures near the root (bottom) of the 7.5-wt.pct. lithium weld of Figure 16, reveals two very distinct morphologies. Closer the weld bottom (right side of picture), the α-Mg phase is oriented approximately parallel to the direction of maximum thermal gradient (i.e. normal to the fusion line) and grew as columnar grains. However the periodicity of this microstructure was rapidly lost after about 100 μm into the weld, where crystal growth orientation appeared to be random, as shown in Figure 18. This columnar microstructure was not observed at the fusion line near the toes of the weld where the fluid flow velocity is higher and the thermal gradient is lower.

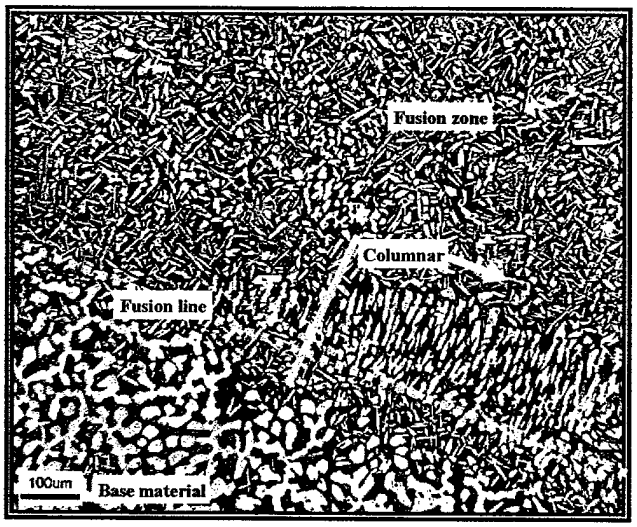

Figure 19. Optical micrograph of the weld fusion line region in the 7.5-wt. pct. lithium alloy

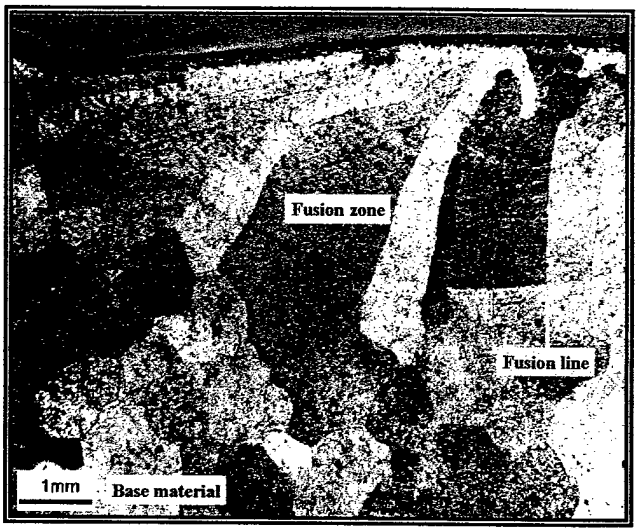

Figure 20. Optical micrograph of half of a weld cross-section in the 10.2-wt.pct. lithium alloy

Figure 20 shows that the single-phase microstructure of the 10.2-wt.pct. lithium alloy is preserved after welding. The grains in the weld fusion zone are particularly large as they stretch over several millimeters from the fusion line to the top of the weld, where solidification ended. The epitaxial growth initiated at the fusion line was clearly not opposed by any undercooling, particularly the undercooling due to composition; an observation that is not surprising in view of the phase equilibria described the equilibrium phase diagram and the initial microstructure seen in Figure 15. Although welding the same material in its work-hardened state could have recrystallized finer grains, the additions of a ternary alloying elements, or even inoculants to promote nucleation and growth of new crystals within the weld pool, may be considered to scale down the solidification microstructure and thus increase strength.

Figure 21 plots results from microhardness indentations at 250-μm spacing across the two welds seen in Figure 16. No major difference between the weld fusion zone and the surrounding base material can be detected, especially for the single-phase 10.2-wt.pct. lithium alloy. Although there are concerns for measurement uncertainties, the small microhardness variations seen in the 10.2-wt.pct. lithium alloy are likely the result of traversing individual grains. When comparing the two materials, the 7.5-wt.pct. lithium alloy is measurably harder than the 10.2-wt.pct. lithium alloy. Welds in the 7.5-wt.pct. lithium alloy were harder due to the fine scale of its phases (large interface densities are effective dislocation barriers) and the presence of the HCP α-Mg phase. Based upon these microhardness results and the absence of microstructural defects (e.g. cracks and pores), strengths of autogeneous weld joints and base materials should be comparable in both alloys.

In conclusion, analysis of autogenous welds on magnesium alloys containing 7.5-wt.pct. lithium and 10.2-wt.pct. lithium has shown areas which will need to be addressed to improve welding. Although the weldability of magnesium-lithium alloys, in terms of defect formation, is excellent compared to other magnesium alloys, work in the areas of microstructural control (grain size, solid-solution and precipitation strengthening, corrosion resistance) and Marangoni flow are suggested. Foreseen ternary additions such as aluminum, calcium, and rare-earth elements will inherently decrease weldability.

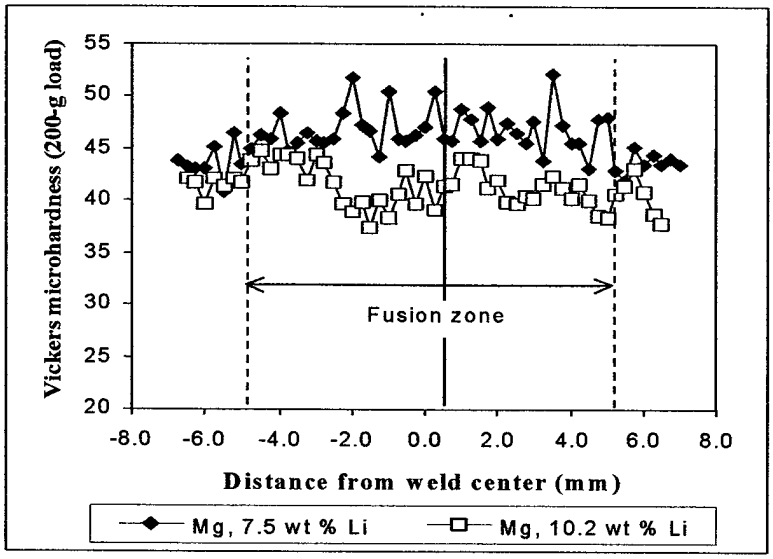

Figure 21. Microhardness indentation results across the welds shown in Figure 5

2.2. Develop Advanced Electronic Property Measurement Techniques for Repair-Weld Assessment

2.2.1. "In Process" Assessment of Weld Microstructure and Properties to be Used as a Quality Control Procedure

Real time assessment of weld microstructure and properties is very important as a quality control tool for field use. The replaced weld microstructure needs to be equivalent to the prior damaged parts microstructure to guarantees the same properties and integrity, which must be met. The preliminary test results of two low carbon steel samples during cooling has been conducted and shown in Figure 21. The probe type of TEP was applied during cooling of the weldments and variation of TEP was observed. A slope discontinuity from the austenite to the ferrite phase transition was observed. This indication suggests that more detailed microstructural changes such as accicular ferrite may be possible to detect during in-progress welding practice and transition time and temperature can be characterized. It can be seen in Figure 21 that as temperature decreases from 900°C to room temperature, the Seebeck coefficient increases and reaches a maximum at the eutectoid temperature (740°C). In addition, the Seebeck coefficient decreases with a further temperature decrease, and hits the minimum value. The minimum peak may indicate that there are some microstructural changes occurring at this temperature, possibly precipitation of minor microstructural constituents such as acicular ferrite. The Seebeck coefficient measurement could be applied to evaluate microstructural constituents occurring during cooling directly after weld solidification. It especially offers a quantitative approach to monitor weld repair on a critical structure and verify that the weld repair achieved the required weld properties.

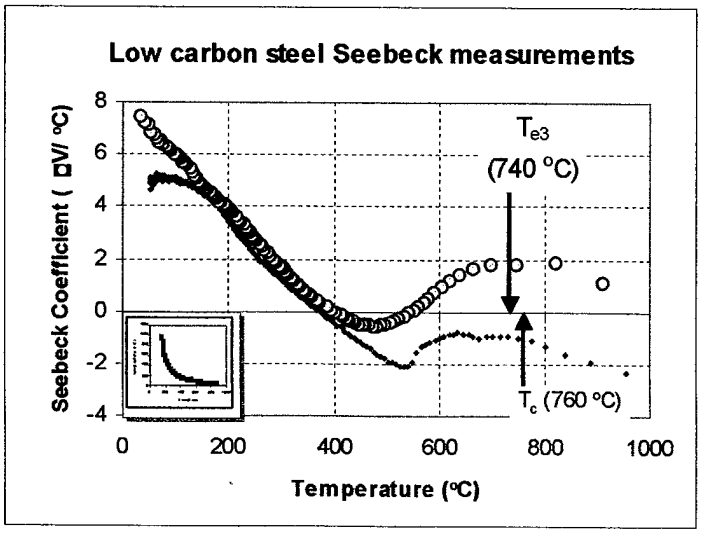

Figure 21 - Preliminary test results of Seebeck (TEP) coefficient on low carbon steel.

TEP measurements across weldments, which have same distance from centerline of weldments, have been performed for GTA welded HSLA steel. First, these results indicate that TEP between weld deposit, heat affected zone, and base metal has distinctive values from each other and can distinguish each zone clearly and all the measurement at different locations across the welds showed similar profiles.

Each weldments, which were welded with different welding current, produced different microstructural constituents, especially in weld metal. Experimental work has been conducted for the TEP coefficient measurement on HSLA steel weld metal microstructure with different welding current levels. The measured TEP coefficients of steel weld metal welded with 100, 120, and 140 Amperes are shown in Figure 22. It appears that the weld metal TEP coefficient of HSLA steel weldments increases as increased welding current is used. Because all other welding parameters were kept constant, increased welding current provides higher heat input, slower cooling rate and a deeper penetrating weld. These different cooling rates result in altered final weld metal microstructure, which are shown in Figure 23. As welding current increases martensitic and bainitic microstructural constituents decrease and accicular ferrite starts to appear at a welding current of 140 Amperes. Since accicular ferrite is more resistant to post weld failure, this approach can be used to ensure the final weld microstructure. Comparing TEP signal profile to final weld microstructure, an investigation is being performed to determine an acceptable TEP signal profile range with repeated experiments. When the TEP coefficient is out of acceptable TEP signal profile during measurement, it is indication of non-preferable microstructural transformation. This technique can be very useful tool for quality control in repair welding because repair weld microstructure should be comparable with a matrix for sound repair welding. Establishment of a calibration procedure must be performed for each steel because each steel has its own characteristic TEP coefficient. By generating databases of TEP signal profile for different microstructural features, this technique can be applied as an easy and accurate quality control device, especially for repair welds.

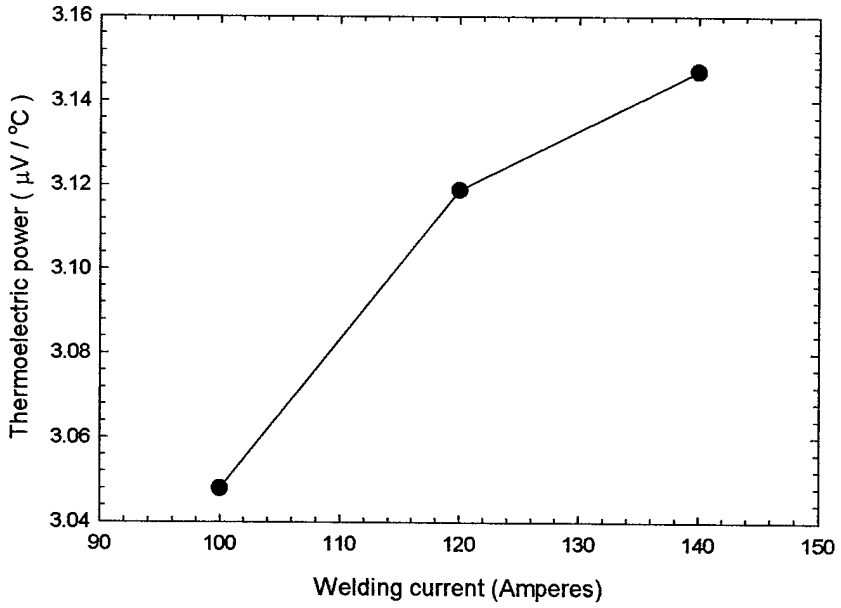

Figure 22 - The measured TEP coefficient across the weldmdments HSLA.

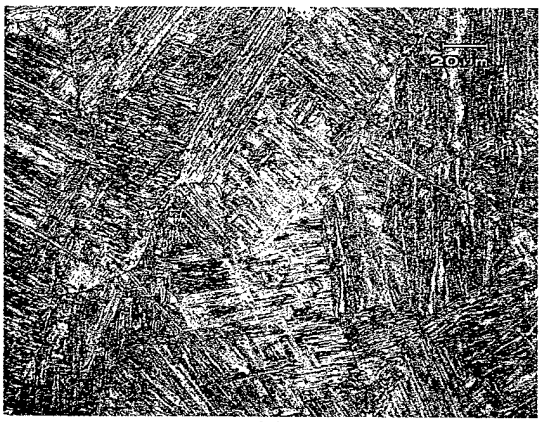

(a)

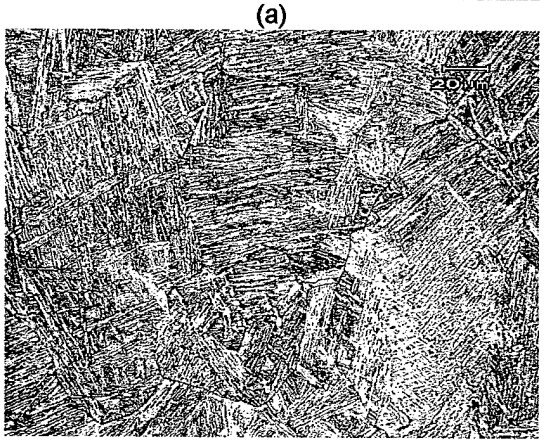

(b)

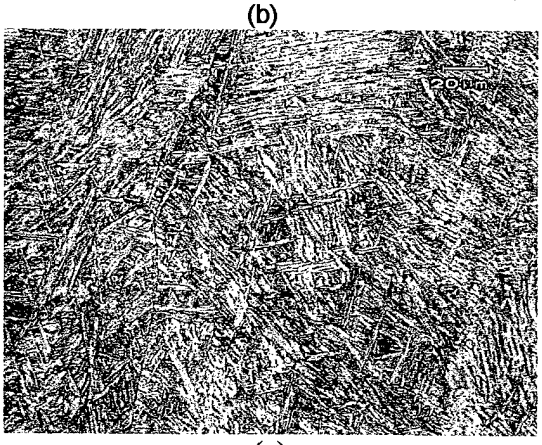

(c)

Figure 23 - Weld metal microstructures of HSLA steel welded with (a) 100 Amperes (mixture of martensite and bainite), (b) 120 Amperes (mostly bainite and little bit of acicular ferrite), and (c) 140 Amperes (mixture of acicular ferrite and grain boundary ferrite). Welding condition: GTAW, 1 mm/sec travel speed, air-cooling.

Also, since hardness is a qualitative indication of the strength of a material, the correlation between TEP and hardness across the weldments offers a direct surface contact electronic property method to assess strength of a weldments. To obtain a more quantitative assessment of the results and to help facilitate comparisons with other parameters, welds were made with different heat input by changing current resulting in various final microstructure. The similar TEP and hardness profile were observed between welds with different heat input. However, lower TEP values were observed in weld deposit with higher heat input.

The comparison of TEP coefficient and Rockwell hardness across the weldments for the HSLA steel welded specimen is shown in Figure 24. The measurement result for specimen welded with 120 Amperes is shown in Figure 24a. The result of both hardness and TEP coefficient for base metal was consistent. The sudden drop in values for both hardness and TEP

coefficient was observed at HAZ. More dramatic change was occurred in TEP coefficient than hardness. In fusion zone, hardness value rose to 28 HRC and was higher base metal because of fast cooling rate after welding. The TEP coefficients of the steel weld metal were higher than those values of HAZ, but lower than base metal. The similar behavior was found in weldments at lower current (80 Ampere) as shown in Figure 24b. Overall, separations of fusion zone, HAZ, and base metal were well obtained from both measurements, but an exact linear relationship was not found between hardness and TEP coefficient. This observation indicated that degree of the variation for TEP coefficient in not correspond to hardness, but the variation in profile across the weldment follows same trends.

Overall, detailed knowledge of mechanical properties (strength, ductility, and hardness), microstructure, and chemical composition needed to be able characterize a weld metal and HAZ. Many NDE techniques which can provide information on any of these features have been developed and is in use. Generally, in contrast to the nondestructive inspection for defects of welds, it is hard to find an approach for nondestructive weldments characterization, which can be applied in a general way. From the point of non destructive Evaluation (NDE) view, the TEP coefficient measurement can be very useful to characterize the weldments by combining with other tests.

a)

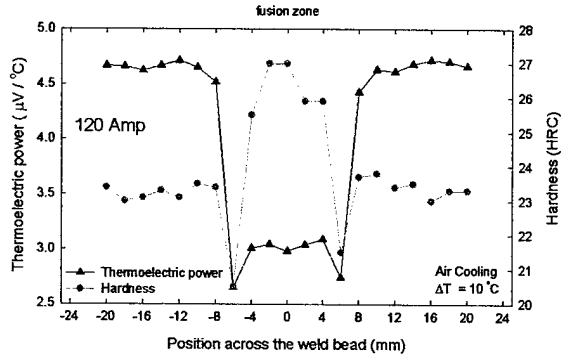

b)

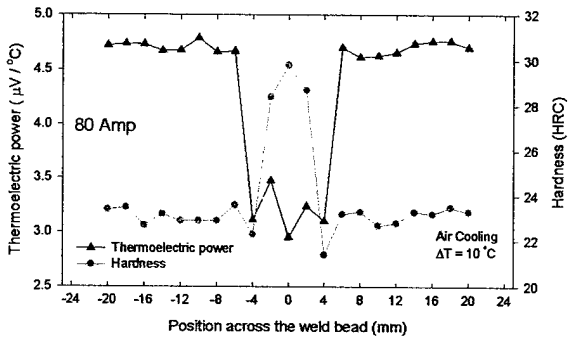

Figure 24. Comparison of TEP coefficients and Rockwell hardness across the weldments for HSLA steel welded specimens.

2.2.2. Use of Thermoelectric Property Measurement as a Method to Assess Residual stress and Nitrogen Content in Nitrogen Strengthened (Non-Magnetic) Stainless Steel

2.2.2.1. Assessment of Residual Stress for weldments of stainless steel.

It is now advantageous to use electronic property measurements Thermoelectric power (TEP) to measure the electronic state of structural alloys to determine the tendency for damage before significant defects arise and to determine residual strain, thus residual stress. To demonstrate a relationship between strain and thermoelectric power an actual strain experiment was conducted while tensile testing and measuring the thermoelectric power coefficient. The experiment was designed to induce elastic strain on a Ni-Al bronze tensile specimen with an Alliance tensile tester, while measuring the TEP coefficient at the same time. A modified TEP coefficient probe measurement set-up was applied to fit a tensile specimen with an attached extensometer. The strain rate used was 0.01 in/min (0.00423 mm/sec) and the gauge length of the specimen is 2 in (50.8 mm). The measured TEP coefficient result as a function of strain is shown in Figure 25. The result indicates that there is linear correlation between the applied strain and the measured TEP coefficient. The scatter in the data can be related to the difficulty in maintaining quality TEP probe contact during tensile testing.

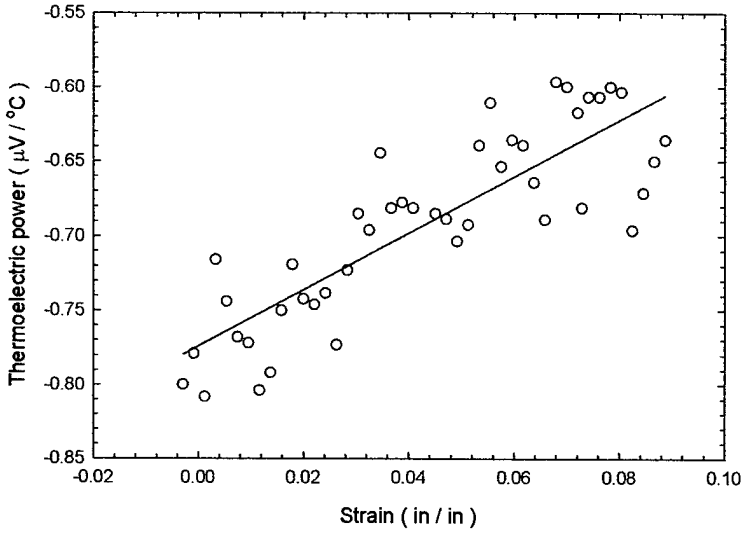

Figure 25 - Measured TEP coefficient as a function of elastic strain for Ni-Al bronze specimen. Tension test condition: strain rate was 0.01 in/min (0.0254 mm), and gauge length was 2 in. (50.8 mm).

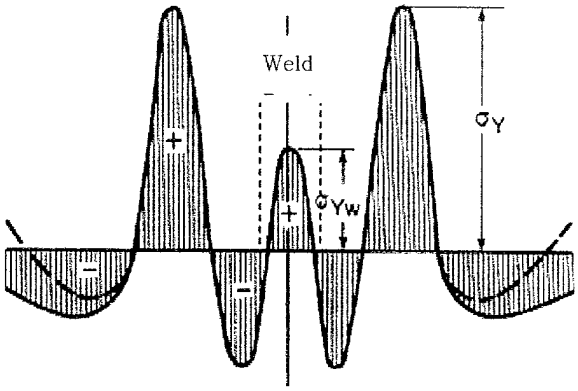

Figure 26 - Weld-longitudinal residual-stresses, stress profile variants: mild steel with austenitic filler metal [18].

The thermoelectric coefficient is a function of the electronic concentration, electronic scattering factor, and the effective mass of the electron. The effective mass of the electron is dependant on the shape of the *sp*- and *d*-bands. It is sensitive to the curvature of the electronic bands where the Fermi energy level contacts them. When the elastic strain is applied to the transition metal alloy such as with the residual stresses from welding (Figure 26), there is a pulling apart or further separation of the overlapping *d*-band, which results in less violation of the Pauli-exclusion principle (no two electrons can exist at the same energy site) resulting in a change in electronic filling of the bands. If strain causes less overlap of the *d*-band then there is a change in the shape of the *d*-band at the Fermi energy level, and thus a change in the effective mass. These changes in the effective mass can be seen by measuring the thermoelectric power coefficient.
Due to the thermal experience of welding, much localized strains result in strains that cause distortion and residual stresses (Figure 26). Welds causes residual stress at a level approaching the yield strength of the base metal. Welding parameters influence the amount and distribution of residual stress because the extent of the stressed region and the amount of distortion is directly proportional to the size of the weld deposit, which in turn is directly related to the heat input. These residual stresses can be important in the generation and propagation of environmentally enhanced cracking. The use of a portable two-probe contact TEP measurement analysis for the determination of residual stress is of particular importance due to its mobility and ease of application.

Research utilized sound scientific approach by systemically changing welding parameters to alter the size of the weld bead. The use of different welding consumables varies the weld thermal expansion coefficients resulting in variations in residual stress in welds. The resulting residual stress conditions were measured and mapped using the thermoelectric power coefficient surface probe measuring technique. The welding of dissimilar metal combinations is also easily assessed utilizing this new technique. By using a number of methods to measure residual stress on these specimens, a calibration practice will be established which will allow for this technique to achieve quantitative residual strain (stress) values. To establish residual stress measurements by using thermoelectric power, welds were performed with identical welding parameters with only a change in the welding speed, which changes the size of the weld pool and thus, the residual stress. The residual stress is being measured by placing the Seebeck probes in the HAZ (within 0.2 mm from the fusion line) of the weldment.

Preliminary residual stress results are shown in Figure 27 (a) and (b) for (German nitrogen strengthened stainless steel alloy 1.4565) welds. Figure 27(a) shows the difference in the Seebeck effect caused by a change in welding speed for GTA welds. Figure 27 (b) shows the difference in Seebeck effect due to change in welding speed for plasma welds. Knowing that a change in the size of the weld bead area affects the residual stress, a schematic change in weld travel speed was used to determine whether the Seebeck effect could be used to determine residual stress. In Figure 27 (a) and (b), the gray color bar indicates a travel speed of 0.1 m/min and the dark gray color bar indicates 0.2 m/min. Figure 27(c) is a schematic diagram of the weld bead and the positioning of the copper probes (yellow circles) for residual stress measurements. A residual stress measurement is made on both sides of the weld in the HAZ for comparison.

An increase in weld travel speed results in a decrease in the area of the weld bead, hence changing the amount of residual stress, which results in an increase in the Seebeck coefficient for both welding processes. These results indicate that the Seebeck coefficient can be used to determine residual stresses resulting from the welding process. Calibration of the Seebeck technique will be performed through residual stress measurements in the HAZ utilizing standard strain tests such as: X-ray diffraction analysis and rosette hole drilling for calibration. This testing will lead to the determination and quantification of the Seebeck coefficient as a function of residual stress associated with the welding process.

(a)

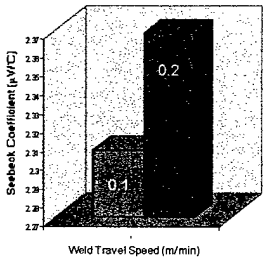

(b)

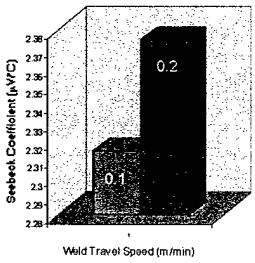

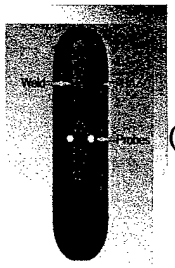

(c)

Figure 27 - Seebeck coefficient as a function of number of weld passes. (a) Difference in Seebeck coefficient in the HAZ of GTAW welds for alloy 1.4565. (b) Difference in Seebeck in the HAZ of Plasma welds for alloy 1.4565. Blue indicates 0.1 m/min and red indicates 0.2 m/min. (c) Schematic diagram of weld indicating hot copper probe position (yellow circles) for residual stress measurements.

2.3 References

1. K. Mitchell, "Cored Wire Repair Welding in the Power Industry", Welding and Metal Fabrication (UK), vol. 66, no. 7, pp. 16-18, 20, Aug. (1998).
2. C.E. Cross, D.L. Olson and S. Liu, "Aluminum Welding", Handbook of Aluminum: editors G.E. Totten and D.S. Mackenzie, Vol (1), "Physical Metallurgy and Processes", pp 481-532, Marcel Dekker, NY (2003).
3. M. Marya, G.R. Edwards, D.L. Olson, "Theoretical Models to Describe Characteristics of Magnesium Alloy Fusion Welds", Proc. of ASM Materials Solutions Conf. And Expo, Int. Conf. On Joining of Advanced Specialty Materials VI, Pittsburgh, PA, Oct. (2003).
4. www.readywelder.com
5. W. Spraragen, G.E. Claussen, "Welding Aluminum and its Alloys by Arc, Torch and Pressure Processes", Welding Journal, Vol. 20, pp 1-38s, Jan. (1941).
6. Penkov, "Properties of Welded Joints in Aluminum in Automatic Welding Under a Fluoride Flux", Weld. Prod. (USSR), 31, (4), 29-30, Apr. (1984).
7. J.L. Jossick, "Flux cored brazing composition", US Patent 5 781 846. Filed: 7 Aug.1995. Publ: 14 July (1998).
8. C.A. Sorrell, J.G. Groetsch Jr, D.M. Soboroff, "Aluminum Fluxing Salts: a Critical Review of the Chemistry and Structures of Alkali Aluminum Halides", Pittsburgh, PA, US Bur. Mines Inf. Circ., #9069, 37 pp, (1986).
9. T.A. Utigard, K. Friesen, R.R. Roy, J. Lim, A. Silny, C. Dupuis, "The properties and uses of fluxes in molten aluminum processing", JOM (USA), 50, (11), 38-43, Nov. (1998).
10. J.C. Benedyk, "Review of Fluxing Fundamentals and Practice in Secondary Aluminum Processing", Light Metal Age, vol. 61, no. 7-8, pp. 22- 31, August (2003).
11. H. Haferdamp, Fr.-W. Bach, P. Juchmann, "New Magnesium-Lithium Alloys of Higher Ductility", Proc. Of Magnesium 2000: Second Israeli International Conference on Magnesium Science & Technology, Edited by E. Aghion, D. Eliezer, Dead Sea, Israel, Potash Publishers, 22-24 Feb. (2000).

12. D.L. Olson, D.W. Wenman, V.I. Kaydanov, C. Suryanarayana, D. Eliezer, "The Search for Room Temperature Cubic Magnesium Alloys", Proc. Of Magnesium 2000: Second Israeli International Conference on Magnesium Science & Technology, Edited by E. Aghion, D. Eliezer, Dead Sea, Israel, Potash Publishers, 22-24 Feb. (2000).

13. Kimura, M., Miyata, Y., Toyooka, T., and Kitahaba, Y., "Effect of Retained Austenite on Corrosion Performance for Modified 13 % Cr Steel Pipe", Corrosion, vol. 57, No. 5, pp 433-439, (2001).
14. Y.D. Park, I. Maroef, A. Landau, and D.L. Olson, "Retained Austenite as a Hydrogen Trap in Steel Welds", Welding Journal, Vol. 81, No. 2, pp 27s-35s, Feb, (2002).
15. Edmondson, B., "Thermal Stabilization of Austenite in 10% Ni, 1% C, steel." Acta Met.,Vol 5, pp 208-215, (1957).
16. John A. Larson, "Retained Austenite and Its Measurements by X-Ray Diffraction", pp 1-3, SAE, Warrendale, PA, (1980).
17. Arnell, R.D.; Ridal, K.A., and Durnin, J., "Determination of Retained Austenite in Steel by X-Ray Diffraction", Journal of Iron Steel Inst, 206 (10), pp.1035- 1036, Oct. (1986).
18. D. Radaj, "Heat Effects of Welding," Springer-Verlag, Berlin, pp 201, (1992).

3.0 ACCOMPLISHMENTS OF THIS RESEARCH CONTRACT PERIOD

- Analysis of autogenous welds on magnesium alloys containing 7.5-wt.pct. Lithium and 10.2-wt.pct. Lithium has shown areas which will need to be addressed to improve weldability. Although the weldability of magnesium-lithium alloys, in terms of defect formation, is excellent compared to other magnesium alloys, work in the areas of microstructural control (grain size, solid-solution and precipitation strengthening, corrosion resistance) and Marangoni flow are suggested. These improvements can result with alloying additions.

- During this contract period the rapid making of specialty metal-cored wires was performed to meet the compositional requirements of defense related alloys for repair welds. This effort determined to correct metal transfer effency for alloying elements in metal powder filled cored welding wires to the weld deposit. This knowledge is essential for accurate selection and use of repair welding consumables.

- The Seebeck coefficient measurements during cooling directly and after weld solidification were applied to evaluate microstructural constituents occurring during welding. It especially provides a quantitative approach to monitor weld repair microstructure on a critical structure, such as accicular ferrite, and verify weather the weld repair is achieved the required weld properties.

- The measurements of TEP coefficient for post-weld microstructure across HSLA steel weldments have shown good correlation with hardness profile and post weld microstructure. These results offer a quality monitoring tool for post weld microstructure evaluation, which is essential for integrity of weldments.

- The volume fraction of retained austenite was determined and correlated well to TEP coefficient measurements for TRIP steels. It was shown that this technique is simple and non-destructive approach to measure Retained austenite volume fraction. Retained austenite must be controlled to achieving reproducible weld properties in the higher strength steels.

- The Seebeck coefficient can be used to determine residual stresses resulting from the welding process. This approach using Seebeck measurement will allow effective way to measure residual stresses in field practice.

4. COLLABORATIONS

In performing our research we maintain collaboration with:

Gregory Vigilante	U.S. Army Benet Laboratories
Dr. Edward Metzbower	U.S. Navy Research Laboratory
Dr. Robert DeNale	U.S. Navy, Naval Surface Warfare Center
Dr. Vinod S. Agarwala	U.S. Navy, Naval Air System Command
Dr. Calvin Hyatt	Canadian Forces, DREA
Dr. Ron Goldfarb	Magnetic Laboratory, NIST, Boulder
Prof. Victor Kaydanov	Electronic Property Measurement Laboratory, Physics Dept., CSM
Dr. Franz Freibert	Los Alamos National Laboratory
Dr. Alex Landau	Israeli Nuclear Center, Beer Sheva, Israel
Dr. Thomas Boellinghaus	BAM (Federal Institute of Materials Research and Testing) Berlin, Germany
Dr. George Wang	Americal Bureau of Shipping
Prof. Dan Eliezer	Ben Gurion University of the Negev, Beer Sheva, Israel
Dr. Manuel Marya	General Motors Research Laboratory

A sub-group research activity to manage corrosion voltage of marine oil tankers (supported by the American Bureau of Shipping and the Royal Thai Navy supplied Naval officers as graduate student) also met with the ARO sponsored research group for their task were very related in scope. Their tasks were to (1) assess advanced non-destructive techniques for rapid identification of locations of corrosion damage and evaluate amount of corrosion wastage of large marine oil Tankers and (2) to perform a statistical study of existing survey reports of 116 tankers to determine the most important locations in the structural components of the Tankers that ship surveyors (inspectors) need to focus on with the short time to assess corrosion damage and to predict the remaining service life or extent of needed repair. These efforts are complimentary to the weld repair and advanced sensing activities of this ARO project. One publication on the assessment of advanced corrosion sensors that are available or soon to be available in listed with accomplishments of the current ARO project.

5. LIST OF PUBLICATIONS FROM THIS RESEARCH CONTRACT PERIOD

(a) Papers published in peer-reviewed journals

1. D.L. Olson, A.N. Lasseigne, M. Marya, and B. Mishra, "Weld Features that Differentiate Weld and Plate Corrosion", "Practical Failure Analysis", Vol 3(5), pp 43-57, October 2003.
2. D.L. Olson, E. Metzbower, S. Liu, and Y.D. Park, "Developments in Property Predictions for Weld Metal", The Paton Welding Journal, 10-11 (2003), pp. 31-37.
3. S. Niyomsoan, W. Grant, D.L Olson, B. Misha. "Variation of color in titanium and zirconium nitride decorative thin films", Thin Solid Films 415(2002) 187-194.
4. P. Termsuksawad, S. Niyomsoan, R.B. Goldfarb, V.I. Kaydanov, D.L. Olson, B. Mishra, Z. Gavra, Measurement of hydrogen in alloys by magnetic and electronic techniques, Journal of Alloys and Compounds 373(2004) 86-95
5. G. Atkins, M. Marya, D.L. Olson, and D. Eliezer, "Magnesium-Lithium Alloy Weldability: A Microstructural Characterization", in Magnesium Technology 2004, pp 37-42, TMS, Warrendale, PA (2004)
6. M. Marya, G.R. Edwards, D.L. Olson, "Fundamentals in the Fusion Welding of Magnesium and Its Alloys", International Symposium of Japan Welding on Today and Tomorrow in Science and Technology of Welding and Joining (20-30 November, 2001,Kobe, Japan)
7. S. Saidarasamoot, D.L. Olson, B. Mishra, J.S. Spencer, and G. Wang, "Assessment of Emerging Technologies for the Detection and Measurement of Corrosion Wastage of Coated Marine Structures", OMAE '03, Proc. of the 22nd Intl. Conference on Offshore Mechanics and Arctic Engineering, Cancun, Mexico, June 8-13, 2003, Paper OMAE 2003-37371, pp 1-11, ASME, NY (2003).

(b) Papers published in non-peer-reviewed journals or in conference proceedings

1. M. Marya, D.L. Olson,V. Kaydanov and S Liu, "Semi-Empirical Correlations and Electronic Model for Thermoelectron Enhancing Particles in GTAW Cathodes", Proc. on Joining of Advanced and Specialty Materials IV, ASM Materials Solution Conference and Exposition, pp. 98-107, November 5-8, 2001, Indianapolis, IN (2002).
2. D. L. Olson, M. Marya, D. W. Wenman, J. D. Olivas, and D. Eliezer, "The Use of Alloying Theory to Enhance the Properties of Magnesium", Proc. of THERMEC '2000, Proceeding of the International Conference on Processing and Manufacturing of Advanced Materials, Las Vegas, NV, Dec 2000: CDROM Section A1, vol. 117/3, Special Issue: J. of Mat. Proc. Techn. , 6 pages, Elsevier Science, UK (October 2001).
3. D.L. Olson, S. Liu, and G.R. Edwards, "Materials Science of Non-Uniform Systems for Interpretation of Weld Metal Behavior", Proc. 7th Intern. Aachener Schweisstechnik Kolloquim, High Productivity Joining Processes: Fundamentals, Applications, and Equipment, vol. II, pp. 831-847, May 3-4, 2001, Aachen, Germany, Shaker Verlag, Germany (2001).
4. C.E. Cross, D.L. Olson and S. Liu, "Aluminum Welding", Handbook of Aluminum: editors G.E. Totten and D.S. Mackenzie, Vol (1), "Physical Metallurgy and Processes", pp481-532, Marcel Dekker, NY (2003).
5. S. Liu and D.L. Olson, "Weld Metal Design: From Flux Coating to Microstructure" in the 6th Conference on the Trends in Welding Research, 15-19 April 2002, Pine Mountain, GA, ASM, Materials Park, pp 529-535, OH (2003).
6. Y.D. Park, A.N. Lasseigne, V.I. Kaydanov, D.L. Olson A. Landau, M. Pinkas, and B. Sarusi, "Thermoelectric Diagnostics for Nondestructive Evaluation of Materials", 10th CF/DRDC MEETING on NAVAL APPLICATIONS OF MATERIALS TECHNOLOGY , CANADA 13-15 May, pp. 648-666 (2003).
7. M. Marya, G.R. Edwards, D.L. Olson, "Theoretical Models to Describe Properties of Magnesium Alloy Fusion Welds", Proceeding of the International Conference on Joining of Advanced and Specialty Materials VI, 2003 ASM Materials Solutions Conference and Exposition, 13-15, October 2003, Pittsburgh, Pennsylvania, USA
8. D.L. Olson, A.N. Lasseigne, M. Marya, and B. Mishra, "Fundamental Models for Corrosion in Fusion Welds-Emphasis on Interfacial and Gradient Effects", Proc. of Joining of Advanced and Specialty Materials V, pp 1-11, ASM 2002 Materials Solution Conf., Columbus, OH, ASM, Materials Park, OH (2003).

(c) Papers presented at meetings, but not published in conference proceedings

1. D.L. Olson, A.N. Lasseigne, M. Marya, B. Mishra and G. Castro, "Materials Science Aspects of Weld Corrosion", Proc. of International Conference on Welding and Joining of Materials, Pontifica Universidad Catolica del Peru, October 27-29, 2003, Lima, Peru (2003).

(d) Manuscripts submitted, but not published

1. Angelique N. Lasseigne, David L. Olson, Thomas Boellinghaus, and Rodney D. Smith, "Non-Destructive Determination of Nitrogen in Nitrogen-Strengthened Austenitic Stainless Steel Weldments Utilizing Thermoelectric Power Coefficient Measurements", International Conference, Ostend, Belgium, Sept. 19-22, 2004.

(e) Technical reports submitted to ARO

6. LIST OF ALL PARTICIPATING SCIENTIFIC PERSONNEL

1. David L. Olson, Professor & Principal Investigator
2. Yeong-Do Park, PhD. Completed Summer 2003
   (Sensing of Weld Microstructure Phase Content and Alloy Stability)
3. Garrett Atkins, (Completed MSci Augest 2004)
   (Light Metal Repair Welding Consumables and Practices)
4. Gerhart Castro MSci student
   (Rapid Manufacturing of Specialty Steel Consumables)
5. Angelique Lasseigne, PhD. Student
   (TEP Analysis for Weld Residual Stress)
6. Ltjg. Swieng Thanboon, MSci Student (Royal Thai Navy), No Cost to ARO
   (Statistical Analysis of Locations for Corrosion on Oil Tankers)
7. Ltjg. Sittha Saidarasamoot, MSci Student (Royal Thai Navy), No Cost to ARO (Assessment of Advanced NDE Techniques to Measure Corrosion on Oil Tankers)